PRAMANA — journal of physics

Vol. 84, No. 1
January 2015
pp. 101–111

On the momentum distribution of particles participating in nuclear stopping

MANDEEP KAUR and SUNEEL KUMAR*

School of Physics and Materials Science, Thapar University, Patiala 147 004, India
*Corresponding author. E-mail: suneel.kumar@thapar.edu

MS received 23 October 2013; revised 22 March 2014; accepted 2 April 2014
DOI: 10.1007/s12043-014-0832-4; ***e*Publication:** 14 September 2014

Abstract. Nuclear stopping is studied as a function of incident energy and charge of the fragment produced in central heavy-ion collisions (HIC) of $^{197}_{79}$Au+$^{197}_{79}$Au and $^{58}_{28}$Ni+$^{58}_{28}$Ni using stopping parameter VARXZ. Various momentum constraints were imposed to get better insight into the stopping. The comparison of measured and calculated values of stopping for protons reveals the significance of these constraints. Maximum stopping is obtained for the particles lying in the lowest range of the momentum distribution at all incident energies.

Keywords. Low and intermediate energy heavy-ion reactions; breakup and momentum distributions.

PACS Nos 25.70.−z; 25.60.Gc

1. Introduction

Central heavy-ion collisions (HIC) provide precious information about the nuclear equation of state (EoS), which virtually reflects the properties of hot and dense nuclear matter under extreme conditions of temperature, pressure and density. These parameters determine the degree of thermalization achieved in a dynamical process during the collision of heavy ions. Several different experimental observables have been proposed in the literature as sensitive probes to study various aspects of nuclear matter at intermediate energies. One of the essential observables, which is necessary to understand the basic reaction dynamics, is the nuclear stopping: a prime source of information for analysing the energy spectra as well as the particle densities of the compressed nuclear matter during the early phase of a reaction when fireball is formed by the participant nucleons [1]. A large fraction of the dissipated energy is governed by the stopping of the nuclear matter. It also constrains the behaviour of nuclear matter at different incident energies and provides information about the EoS, nucleon–nucleon (N–N) cross-section and degree of equilibration reached in a heavy-ion collision. Zhang *et al* [2] suggested that in statistical average, it is quite difficult to achieve equilibrium state near the Fermi energy, even

for the central HIC. Bauer *et al* [3] pointed out that the nuclear stopping power is calculated using both mean field as well as in-medium nucleon–nucleon cross-section. Note that, the symmetry potential was not included in their study. Later on Bass, Yennello and Johnston [4] suggested that the degree of approaching isospin equilibration provides a powerful probe to determine the mechanism behind the nuclear stopping. In [5], sensitivity of the nuclear stopping was checked with reference to the isospin dependence of binary cross-section. Recently, Zhang *et al* [6] pointed out that the stopping observables depend strongly on the *N–N* cross-section and mean field, whereas the flow observables depend comparatively on the uncertainties in the *N–N* cross-section and mean field. Kumar *et al* studied the effect of different EoS and *N–N* cross-section on nuclear stopping and found it to be highly sensitive towards the *N–N* cross-section and weakly towards different EoS [7,8]. Despite these observations, there are further ambiguities associated with the nuclear EoS. This being the case, it is important to constrain the specific observables to limit the uncertainties in the nuclear EoS.

Interestingly, momentum distribution of the fragments has rarely been studied, though it can shed light on the reaction mechanism. Peilert *et al* [9] investigated the equilibration of the incident longitudinal momentum in *N–N* collisions and found that just after the stage of maximum compression, the matter flows out of the central zone and causes degradation of the longitudinal momenta into transverse degree of freedom. They also pointed out that for achieving a better thermalization, one should consider the participant region only. Ono *et al* [10] have studied the momentum distribution of the fragments produced in the reaction of $^{12}C+^{12}C$ at an incident energy of 28.7 MeV/nucleon by considering several cases of stochastic collisions. They found that the momentum distribution is sensitive to the stochastic collision process. They also found that collective flow of low-momentum particles (such as α-particles) seems to reflect the effective interactions compared to the flow of free nucleons alone.

Chung *et al* [11] investigated the proton elliptic flow at different colliding geometries by implementing various momentum constraints for the reaction of $^{197}_{79}Au + {}^{197}_{79}Au$ and found that these constraints provide a better understanding of the interplay between hot and compressed nuclear matter. Therefore, it would be interesting to investigate the nuclear stopping associated with the nucleons having different momentum.

Here, we present precise and selective study of the nuclear stopping by constraining the momentum distribution of the particles participating in nuclear reactions. The main purpose of this paper is to investigate which momentum range of the particles is contributing significantly towards nuclear stopping at a particular energy and impact parameter. The present simulations have been carried out within the framework of isospin-dependent quantum molecular dynamics (IQMD) model [12,13] explained in §2.

2. Isospin-dependent quantum molecular dynamics (IQMD) model

The IQMD model along with the QMD version has been quite successful in explaining various phenomena such as collective flow, fragmentation and elliptical flow [7,12–18]. The symmetry potential, Coulomb interaction and cross-section collectively give rise to the isospin degree of freedom to be implemented in the calculations of our results. The details of the elastic and inelastic cross-sections for proton–proton and

neutron–neutron collisions can be found in [12]. In IQMD model, the nucleons of the target and projectile interact via two- and three-body Skyrme forces, Yukawa potential and Coulomb interactions. In addition to the use of explicit charge states of all baryons and mesons, a symmetry potential between protons and neutrons corresponding to the Bethe–Weizsacker mass formula has been included. The hadrons propagate using Hamilton equations of motion:

$$\frac{\mathrm{d}\vec{r}_i}{\mathrm{d}t} = \frac{\partial\langle H\rangle}{\partial p_i}; \qquad \frac{\mathrm{d}\vec{p}_i}{\mathrm{d}t} = -\frac{\partial\langle H\rangle}{\partial r_i} \tag{1}$$

with

$$\begin{aligned}\langle H\rangle &= \langle T\rangle + \langle V\rangle \\ &= \sum_i \frac{p_i^2}{2m_i} + \sum_i \sum_{j>i} \int f_i(\vec{r},\vec{p},t) V^{ij}(\vec{r}',\vec{r}) \\ &\quad \times f_j(\vec{r}',\vec{p}',t)\mathrm{d}\vec{r}\mathrm{d}\vec{r}'\mathrm{d}\vec{p}\mathrm{d}\vec{p}'.\end{aligned} \tag{2}$$

The baryon–baryon potential V^{ij}, in the above relation, reads as

$$\begin{aligned}V^{ij}(\vec{r}'-\vec{r}) &= V^{ij}_{\mathrm{Skyrme}} + V^{ij}_{\mathrm{Yukawa}} + V^{ij}_{\mathrm{Coul}} + V^{ij}_{\mathrm{sym}} + V^{ij}_{\mathrm{mdi}} \\ &= \left(t_1\delta(\vec{r}'-\vec{r}) + t_2\delta(\vec{r}'-\vec{r})\rho^{\gamma-1}\left(\frac{\vec{r}'+\vec{r}}{2}\right)\right) \\ &\quad + t_3\frac{\exp(|\vec{r}'-\vec{r}|/\mu)}{(|\vec{r}'-\vec{r}|/\mu)} + \frac{Z_iZ_je^2}{|\vec{r}'-\vec{r}|} \\ &\quad + t_4\frac{1}{\varrho_0}T_3^iT_3^j\delta(\vec{r}'-\vec{r}) \\ &\quad + t_5\ln^2[t_6(\vec{p}'-\vec{p})^2+1]\delta(\vec{r}'-\vec{r}).\end{aligned} \tag{3}$$

Here Z_i and Z_j denote the charges of ith and jth baryons. The parameters μ and $t_1,\ldots,t_6$ are adjusted to the real part of the nucleonic optical potential. The momentum-dependent interactions can be incorporated by parametrizing the momentum dependence of the real part of the optical potential [19]. The phase space of nucleons is analysed by using the clusterization algorithm. The widely used clusterization algorithm is the minimum spanning tree (MST) method [16,17]. In the MST method, two nucleons are allowed to share the same fragment if their centroids are closer than a distance $r_{\min}$

$$|r_i - r_j| \le r_{\min}, \tag{4}$$

where r_i and r_j are the spatial positions of both nucleons. The value of $r_{\min}$ can vary between 2 and 4 fm.

3. Results and discussion

For the present analysis, we simulated several thousand events for the reactions of $^{197}_{79}$Au+$^{197}_{79}$Au and $^{58}_{28}$Ni+$^{58}_{28}$Ni at reduced impact parameter $\hat{b} < 0.15$, where $\hat{b} = b/b_{\max}$ with $b_{\max} = 1.15(A_1^{1/3} + A_2^{1/3})$, A_1 and A_2 being the masses of the target and the projectile, respectively. The choice of impact parameter is guided by the experimental

measurements [20]. Simulations were carried out for the incident energies ranging between 50 and 1000 MeV/nucleon. A soft EoS along with $0.8\sigma_{nn}^{\text{free}}$ has been employed that also includes the standard symmetry potential (for more clarity, reader is referred to [12]). The reactions are followed until the saturation is reached, which in the present work is 200 fm/c. The phase space of nucleon was tested before and after binary collisions for a large number of events and on an average, a change in momentum of a few hundreds of MeV/c was found.

In order to explore the participation of nucleons in stopping with a specific momentum, we divide the whole momentum range into different bins MBIN(I), MBIN(II), MBIN(III), MBIN(IV) and MBIN(V). The momentum ranges of different bins are listed in table 1.

It is worth mentioning that various observables have been mentioned in the literature to probe the nuclear stopping [20,21]. One of these observables involves the ratio of variances of transverse rapidity distribution to the longitudinal rapidity distribution, denoted by VARXZ, where the longitudinal rapidity distribution is given by the relation [22]

$$Y(i) = \frac{1}{2} \ln \frac{E(i) + P_z(i)c}{E(i) - P_z(i)c}, \tag{5}$$

where $E(i)$ and $P_z(i)$ are, respectively, the total energy and longitudinal momentum of the ith particle. In order to get the transverse rapidity distribution, the longitudinal component of the momentum (P_z) is replaced by the transverse component of the momentum (P_x).

Now, the stopping observable, VARXZ, is the ratio of variances of transverse (VARX or $\sigma^2(x)$) relative to the longitudinal (VARZ or $\sigma^2(z)$) rapidity distribution.

$$\text{VARXZ} = \frac{\sigma^2(x)}{\sigma^2(z)}; \qquad \sigma^2(x) = (\text{FWHM}/2.36)^2. \tag{6}$$

In order to study the momentum distribution of charge fragments, we display in figure 1, the momentum distribution of the particles as a function of incident energy for the central collisions of the reaction $^{197}_{79}$Au+$^{197}_{79}$Au at 200 fm/c. It is clear from the figure that the percentage of particles lying within the lowest momentum range (MBIN(I)) is less compared to all other momentum range bins at energies $\geq$200 MeV/nucleon. The momentum distribution of the particles of MBIN(I) is followed by MBIN(II) and then by MBIN(III) and finally by MBIN(IV). Moreover, one can clearly see that below 400 MeV/nucleon, the momentum transferred to the particles is not uniform. For MBIN(I) and MBIN(II), it decreases with increase in the incident energy, whereas for MBIN(III) and MBIN(IV) the number of particles increases upto 200 MeV/nucleon (400 MeV/nucleon) for MBIN(III) (MBIN(IV)) and then decreases with further increase

Table 1. Momentum ranges for different momentum bins.

Bin	Momentum range (MeV/c)
MBIN(I)	$0 < p \leq 100$
MBIN(II)	$100 < p \leq 200$
MBIN(III)	$200 < p \leq 300$
MBIN(IV)	$300 < p \leq 400$
MBIN(V)	$p > 400$

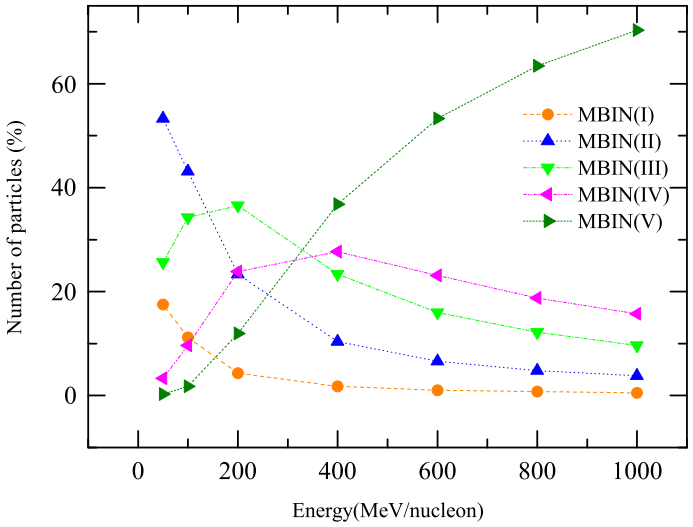

Figure 1. Momentum distribution of particles as a function of incident energy using various momentum cuts MBIN(I), MBIN(II), MBIN(III), MBIN(IV) and MBIN(V).

in incident energy. The distribution of the particles belonging to MBIN(I) remains nearly the same at an incident energy $\geq$200 MeV/nucleon, whereas, that of particles lying in MBIN(II) and MBIN(III), keep on decreasing with increase in incident energy beyond 200 MeV/nucleon. After 400 MeV/nucleon, there is a significant increase in the number of particles in higher momentum range bins. With the increase in incident energy, there is an increase in the binary $N-N$ collisions. Hence, the nucleons with low momenta associated with them get accelerated towards the high-momentum bin, thereby creating a vacancy in the lower-momentum bin. So with an increase in incident energy, the number of particles in lower-momentum bin decreases and those in the higher-momentum bin increases simultaneously. Although we have considered the complete range of incident energy, the main aim of this paper is confined upto 400 MeV/nucleon. Above 400 MeV/nucleon, due to the complete disassembly of nuclear matter, the nuclear stopping decreases and transparency comes into picture. In the following discussion, we mainly concentrate on the results at incident energy below 400 MeV/nucleon.

Figure 2 shows the stopping parameter VARXZ as a function of Z at different incident energies for the reactions $^{197}_{79}$Au+$^{197}_{79}$Au and $^{58}_{28}$Ni+$^{58}_{28}$Ni. It is worth mentioning that, for calculating VARXZ, the rapidity distribution of nucleons is fitted over the entire rapidity range (i.e. $-1.75 \leq (Y_{\text{c.m.}}/Y_{\text{beam}}) \leq 1.75$). The figure shows the stopping ratio for the selected momentum bins and the whole range of momentum distribution (M-ALL). The following conclusions can be drawn from the figure:

(1) It is clear from the figure that the stopping ratio decreases with the increase in fragment charge. With increase in fragment charge, the longitudinal component of rapidity distribution increases compared to the transverse rapidity distribution. Due to this reason there is anisotropic distribution of nucleons in the momentum space. Similar results are also shown in [20].

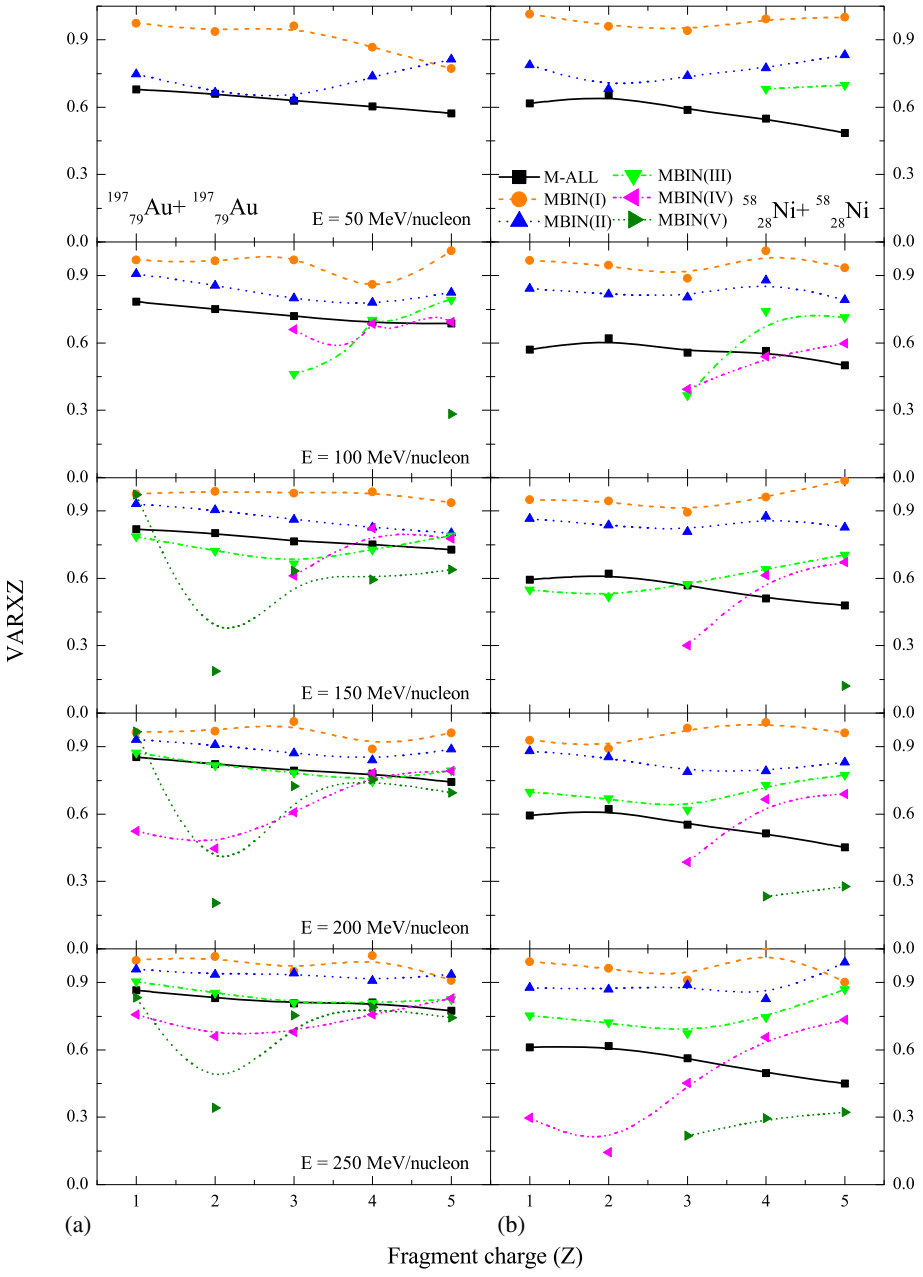

Figure 2. VARXZ as a function of charge of fragment (Z) for (**a**) $^{197}_{79}$Au+$^{197}_{79}$Au and (**b**) $^{58}_{28}$Ni+$^{58}_{28}$Ni at various incident energies and momentum bins.

(2) One can clearly observe that stopping is maximum for MBIN(I) particles. This is due to the dominance of the participant zone. Particles with small momentum accumulate near the mid-rapidity region and yield a compressed participant zone and

hence result in larger nuclear stopping. As we move towards the high-momentum range associated with the particles, the dominance of the participant region starts decreasing. Particles with large momentum tend to increase the longitudinal component of the rapidity compared to the transverse component. Moreover, as we consider the whole momentum range of the colliding nucleons (M-ALL), the overall nuclear stopping decreases.

(3) A closer look at figure 2 shows that at low incident energies, particles with large momentum are not available to take part in the nuclear stopping, but with an increase in the incident energy, high-momentum particles also start participating initially for the heavier fragments and then for all the fragments. In addition, the stopping ratio does not follow a uniform trend with an increase in the charge of fragments for all momentum bins and there is a large variation in the stopping ratio with increase in the fragment charge for the highest momentum bin (MBIN(IV)). Similar trend is also observed for the reaction $^{58}_{28}$Ni+$^{58}_{28}$Ni. It is worth mentioning here that the high momentum particles tend to decrease the stopping ratio due to the broader shape of longitudinal rapidity distribution. Therefore, a minimum in stopping ratio is observed around $Z = 2$ fragment.

Figure 3 displays the stopping ratio VARXZ as a function of incident energy for the selected range of momentum bins. A slight increase in the stopping ratio with increase in incident energy is observed for all momentum bins. The argument is true for all the fragments irrespective of the reactions considered. It also confirms the previous findings that MBIN(I) particles contribute maximum towards stopping. With an increase in incident energy, one expects a progressive increase in *N–N* collisions at the expense of the nuclear mean field. Due to this, there is a rapid increase in the transverse energy, that enhances stopping in the longitudinal direction. For the light charge fragments, particles with large momenta are available only at high incident energies, whereas, for the heavy charge fragments ($Z \geq 3$) particles with large momentum exist throughout the energy range. Comparison of the results for the reactions $^{197}_{79}$Au+$^{197}_{79}$Au with $^{58}_{28}$Ni+$^{58}_{28}$Ni reveals that less stopping is observed for the lighter systems. This is due to the fact that stopping is governed by the participant zone only and depends on the mass of the colliding nuclei. Moreover, for lighter systems, the distance between two successive collisions is comparable to the diameter of the nucleons. This results in more transparency.

Figure 4 shows the stopping ratio as a function of momentum distribution of the particles. Results are plotted at the higher limit of each momentum bin. Various symbols indicate different incident energies. Panels from top to bottom indicate the stopping ratio for different fragments of $^{197}_{79}$Au+$^{197}_{79}$Au (figure 4a) and $^{58}_{28}$Ni+$^{58}_{28}$Ni (figure 4b). One can clearly see that stopping ratio decreases with increase in the momentum associated with the particles. This is because, at saturation time of a reaction, the charge fragments with large momentum move away from the participant zone and contribute the least in nuclear stopping.

Finally, we show the sensitivity of the free protons with a specific momentum towards nuclear stopping as a function of incident energy. One can clearly see that, at low incident energies ($\leq$ 400 MeV/nucleon) nuclear stopping increases with incident energy for all the momentum distribution (M-ALL) taken into account, whereas for a specific range of momentum distribution, there is a sharp increase in the stopping ratio upto 400 MeV/

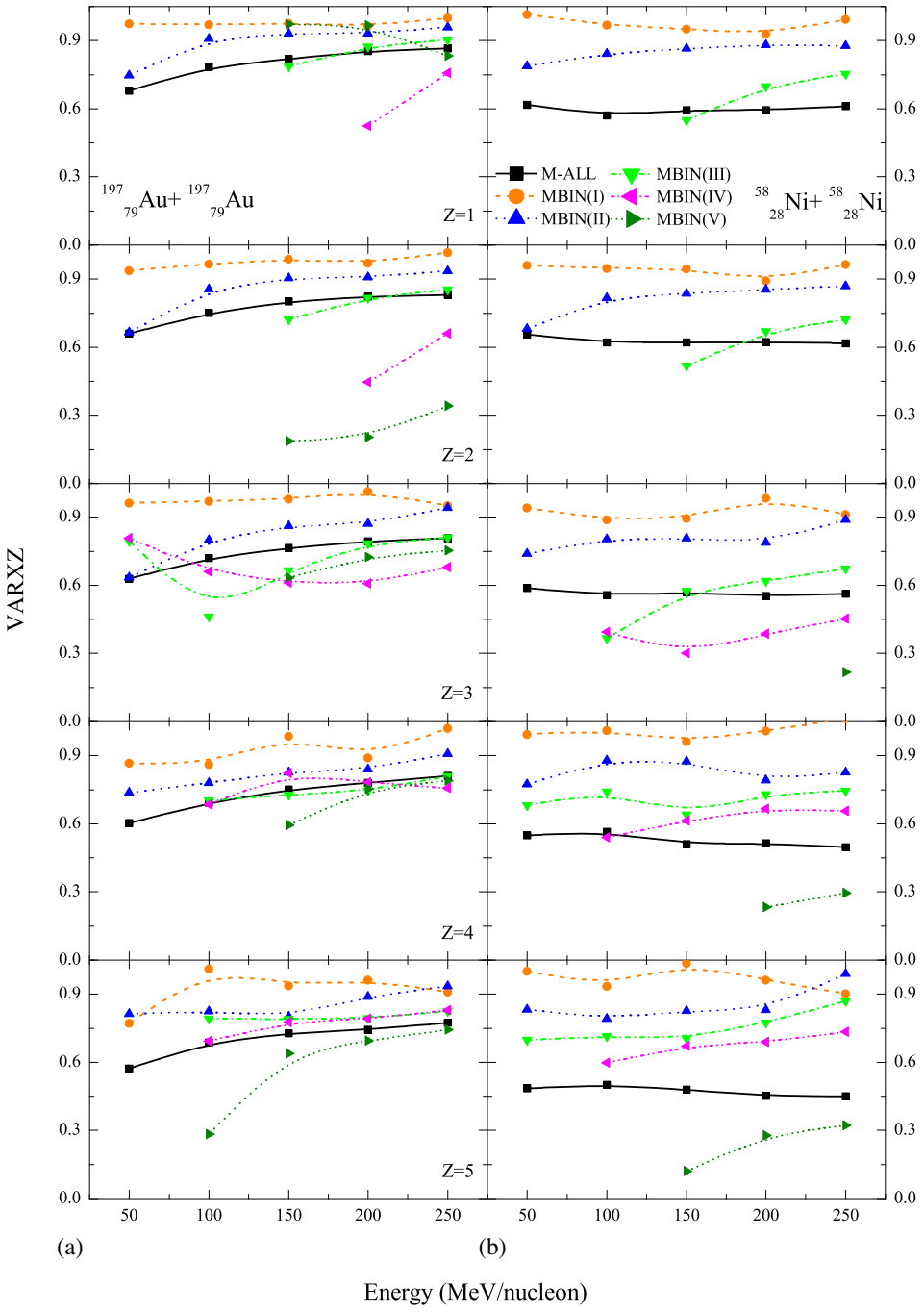

Figure 3. VARXZ as a function of incident energy for (**a**) $^{197}_{79}$Au+$^{197}_{79}$Au and (**b**) $^{58}_{28}$Ni+$^{58}_{28}$Ni for different Z and momentum bins defined in table 1.

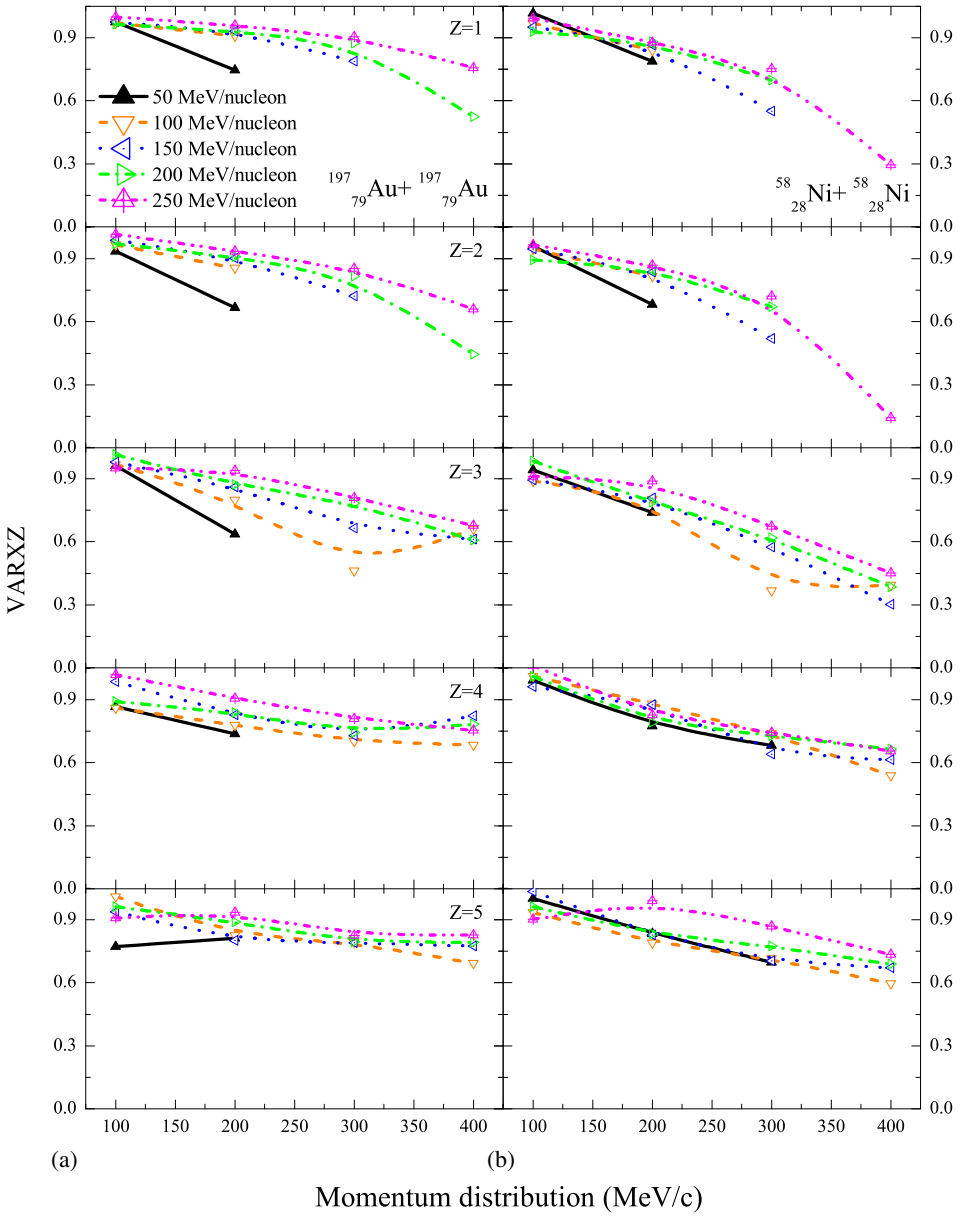

Figure 4. VARXZ as a function of momentum associated with the fragments.

nucleon. After this energy, there is a slight variation in the stopping ratio. These results are in agreement with the findings of Reisdorf *et al* [23] that maximum stopping is observed at 400 MeV/nucleon. For the verification of our results, we have also compared our calculations with the available experimental data [20]. A closer look at figure 5 indicates that at low incident energies, fragments contributing to nuclear stopping lie in MBIN(I)

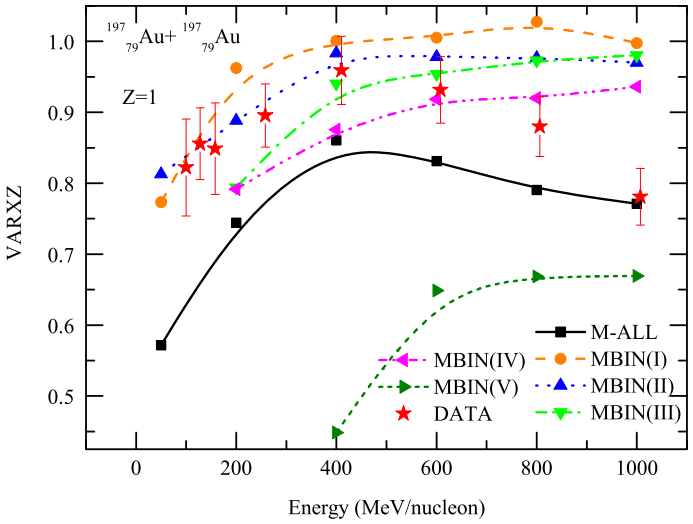

Figure 5. VARXZ as a function of incident energy for free protons of the system $^{197}_{79}$Au+$^{197}_{79}$Au.

and MBIN(II) bins. With an increase in the incident energy, the momentum range of the fragments also shifts towards the higher end. Upto 600 MeV/nucleon, the fragments causing nuclear stopping lies in the bins MBIN(II), MBIN(III) and MBIN(IV). Above 600 MeV/nucleon, higher momentum bin particles play dominant roles in nuclear stopping. At 1000 MeV/nucleon, there are lesser number of fragments carrying high momentum which contribute in nuclear stopping.

Although the fragments lying in the higher-momentum bins contribute more, their contribution in nuclear stopping is the least. The comparison of theoretical calculations with the experimental data indicates that average effect of all the momentum distributions follows a similar trend as recorded by the experimental data.

4. Conclusion

To summarize, using the IQMD model, nuclear stopping is studied by imposing momentum constraints. Comparison of our results with experimental data reveals that at a particular incident energy, a significant number of particles having a specific momentum are produced and maximum stopping is observed for the lowest range of momentum distribution considered. Moreover, for all the momentum distribution taken into account, the nuclear stopping first increases sharply upto 400 MeV/nucleon and then decreases slightly with increase in incident energy.

Acknowledgements

This work is supported by the grant from UGC, Govt. of India (Grant no. F1-17.1/2012-13/ MANF-2012-13-SIK-PUN-9214).

References

[1] B Hong *et al*, *Phys. Rev. C* **66**, 034901 (2002)
[2] G Q Zhang *et al*, *Phys. Rev. C* **84**, 034612 (2011)
[3] W Bauer, *Phys. Rev. Lett.* **61**, 2534 (1988)
[4] B A Li and S J Yennello, *Phys. Rev. C* **52**, 1746 (1995)
S A Bass *et al*, *GSI Scientific Report*, 66 (1994)
H Johnston *et al*, *Phys. Lett. B* **371**, 186 (1996)
S J Yennello *et al*, *Phys. Lett. B* **321**, 15 (1994)
[5] J Y Liu *et al*, *Phys. Rev. Lett.* **86**, 975 (2001)
[6] Y Zhang, Z Li and P Danielewicz, *Phys. Rev. C* **75**, 034615 (2007)
[7] S Kumar, S Kumar and R K Puri, *Phys. Rev. C* **81**, 014601 (2011)
[8] A Jain, S Kumar and R K Puri, *Phys. Rev. C* **84**, 057602 (2011)
[9] G Peilert, H Stöcker and W Greiner, *Rep. Prog. Phys.* **57**, 533 (1994)
[10] A Ono *et al*, *Phys. Rev. C* **47**, 2652 (1993)
[11] P Chung *et al*, *Phys. Rev. C* **66**, 021901(R) (2002)
[12] C Hartnack *et al*, *Eur. Phys. J. A* **1**, 151 (1998)
[13] C Hartnack, H Oeschler, Y Leifels, E L Bratkovskaya and J Aichelin, *Phys. Rep.* **510**, 119 (2012)
[14] S Gautam, A D Sood, R K Puri and J Aichelin, *Phys. Rev. C* **83**, 034606 (2011)
R Bansal, S Gautam, R K Puri and J Aichelin, *Phys. Rev. C* **87**, 061602(R) (2013)
S Gautam and R K Puri, *Phys. Rev. C* **85**, 067601 (2012)
S Gautam, A D Sood, R K Puri and J Aichelin, *Phys. Rev. C* **83**, 014603 (2011)
[15] S Gautam, R Chugh, A D Sood, R K Puri, C Hartnack and J Aichelin, *J. Phys. G: Nucl. Part. Phys.* **37**, 085102 (2010)
S Gautam, A D Sood, R K Puri and J Aichelin, *Phys. Rev. C* **83**, 014603 (2011)
R Chugh and R K Puri, *Phys. Rev. C* **82**, 014603 (2010)
S Kumar, M K Sharma and R K Puri, *Phys. Rev. C* **58**, 3494 (1998)
[16] R K Puri, C Hartnack and J Aichelin, *Phys. Rev. C* **54**, R28 (1996)
R K Puri and J Aichelin, *J. Comp. Phys.* **162**, 245 (2000)
S Goyal and R K Puri, *Phys. Rev. C* **83**, 047601 (2011)
[17] S Kumar, S Kumar and R K Puri, *Phys. Rev. C* **78**, 064602 (2008)
S Kaur and R K Puri, *Phys. Rev. C* **87**, 014620 (2013)
Y K Vermani, S Goyal and R K Puri, *Phys. Rev. C* **79**, 064613 (2009)
Y K Vermani, S Goyal and R K Puri, *Euro. Phys. Lett.* **85**, 62001 (2009)
Y K Vermani, J K Dhawan, S Goyal, R K Puri and J Aichelin, *J. Phys. G: Nucl. Part. Phys.* **37**, 015105 (2010)
Y K Vermani and R K Puri, *J. Phys. G: Nucl. Part. Phys.* **36**, 105103 (2009)
[18] S Kumar, S Kumar and R K Puri, *Phys. Rev. C* **81**, 014611 (2010)
V Kaur, S Kumar and R K Puri, *Phys. Lett. B* **697**, 512 (2011)
K S Vinayak and S Kumar, *Eur. Phys. J. A* **47**, 144 (2011)
[19] J Aichelin *et al*, *Phys. Rev. Lett.* **58** 1926 (1987)
[20] W Reisdorf, *et al*, *Nucl. Phys. A* **848**, 366 (2010)
[21] G Lehaut *et al*, *Phys. Rev. Lett.* **104**, 232701 (2010)
[22] J Aichelin, *Phys. Rep.* **202**, 233 (1991)
[23] W Reisdorf *et al*, *Phys. Rev. Lett.* **92**, 232301 (2004)